Available online at www.sciencedirect.com
SCIENCE DIRECT®
Vision Research 44 (2004) 2643–2652
Vision Research
www.elsevier.com/locate/visres

The absorption of polarized light by vertebrate photoreceptors

N.W. Roberts *, H.F. Gleeson

Department of Physics and Astronomy, University of Manchester, Manchester M13 9PL, UK

Received 26 April 2004; received in revised form 9 June 2004

Abstract

A physiologically realistic model has been constructed for a theoretical study of the mechanisms by which the vertebrate visual system absorbs linearly polarized light. Using a 4×4 matrix technique, analytic solutions to Maxwell's equations have been deduced for rod and cone photoreceptors, allowing calculation of the absorbance as a function of wavelength for a variety of illumination geometries. With the use of experimentally measured optical parameters, the calculated absorbance spectra show excellent agreement in both magnitude and form with microspectrophotometric data. Moreover, failing to correct for the true nature of reflection or scattering in the sample, results in the elevated absorbance commonly seen at shorter wavelengths in experimental measurements. Finally, calculated dichroic ratios also accurately predict experimental results, mirroring the differences seen between rods and cones.

Abbreviations: UVS, ultra-violet sensitive; SWS, short-wavelength sensitive; MWS, mid-wavelength sensitive; LWS, long-wavelength sensitive
Keywords: Vertebrate photoreceptors; Optical modelling; Birefringence; Linear dichroism; Absorbance spectra; Microspectrophotometry

1. Introduction

The optical properties of rod and cone photoreceptors depend strongly on their birefringent and dichroic structure. Order at the molecular level and the photoreceptor's anisotropic structure defines how light is absorbed by these highly specialized cells (Harosi, 1981; Snyder, 1979). For example, it is now almost 70 years since Schmidt (1938) discovered that light was absorbed more strongly when polarized parallel to the transverse axis of the photoreceptor outer segment. He correctly interpreted this dichroism as evidence for the transverse orientation of the chromophore, something which has since been confirmed by other workers (Harosi, 1975; Harosi & Malerba, 1975; Liebman, 1962).

Experimental measurements of the photoreceptors' optical structure very quickly generated the need for a quantitative interpretation of the results within a theoretical framework. Both Denton (1958) and Liebman (1962) recognized this, and by analyzing the ratio of the absorbance of light polarized parallel and perpendicular to the transverse axis of the photoreceptor (the dichroic ratio), it was soon discovered that the main transition dipole moment of the chromophore was tilted with respect to the transverse axis of the outer segment. Harosi and Malerba (1975) further improved on this treatment, theoretically investigating how high numerical apertures within the experimental apparatus affected the analysis of results, and producing a generalized model of dichroic absorption. An alternate theoretical direction (Liebman, Jagger, Kaplan, & Bargoot, 1974; Weale, 1971) has also been followed in terms of relating the measured birefringence of photoreceptor outer segments to both the ultra-structure of the cell and the anisotropic nature of the membranes. Liebman (1975), Laughlin, Menzel, and Snyder (1975) and Harosi (1981) have all provided reviews on the analysis of birefringence measurements by considering the optics of

* Corresponding author. Tel.: +44 161 2754236.
E-mail address: nickr@reynolds.ph.man.ac.uk (N.W. Roberts).

0042-6989/$ - see front matter © 2004 Elsevier Ltd. All rights reserved.
doi:10.1016/j.visres.2004.06.001

model anisotropic systems. However, no work has yet unified these two different directions, providing a model for calculating the spectral absorbance and dichroic ratios of vertebrate photoreceptors within an optically and physiologically accurate framework.

It is this unification we address in the current work. By considering optical parameters such as the real and complex parts of the refractive indices, intrinsic and form birefringence and physical parameters such as rotational diffusion, we derive the complex dielectric tensor for a vertebrate photoreceptor. Furthermore, by applying a well proven technique from the field of liquid crystal physics (Berreman, 1972), we use this dielectric tensor to calculate both the transverse and axial spectral photoreceptor absorbance from analytic solutions to Maxwell's equations. We believe this is the first instance where this technique from liquid crystal physics, a topic intrinsically concerned with the optics of anisotropic systems, has been applied to this area of vision research. The well proven basis of the theory (Azzam & Bashara, 1987; Berreman, 1972; Roberts et al., 2003; StJohn, Fritz, Lu, & Yang, 1995) allows us to make valid and direct comparisons between our theoretical calculations and previously published experimental absorbance spectra and dichroic ratio measurements.

2. The photoreceptor dielectric tensor

The optics of complex anisotropic structures are commonly modelled using a 4×4 matrix technique (Berreman, 1972). The method allows analytic solutions of Maxwell's equations to be deduced and the transmitted and reflected intensities calculated for the system being modelled here. The absorbance of the system, A, can then be calculated using the formula (Harosi, 1981)

$$A = \log_{10}\frac{I_R}{I_M}, \tag{1}$$

where I_R is the light intensity incident on the photoreceptor (reference measurement) and I_M is the intensity transmitted by the photoreceptor. Indeed, there are strong parallels between the structure of some liquid crystal phases and the self-assembling membrane structures that constitute the outer segments of rods and cones, confirming the validity of our approach. The ordered stacks of photopigment-containing membranes within the outer segment are a model example of the lamellar liquid crystal phase. To calculate the absorbance of the anisotropic layered structure for both rods and cones, the complex dielectric tensor must first be derived for these individual anisotropic bilayers. The following derivation will initially consider the situation of a single photoreceptor being illuminated from the side, this being the illumination geometry used in all experimental measurements to date. The coordinate system, a representation of the complex dielectric tensor to be derived and angles to be used are detailed in Fig. 1A.

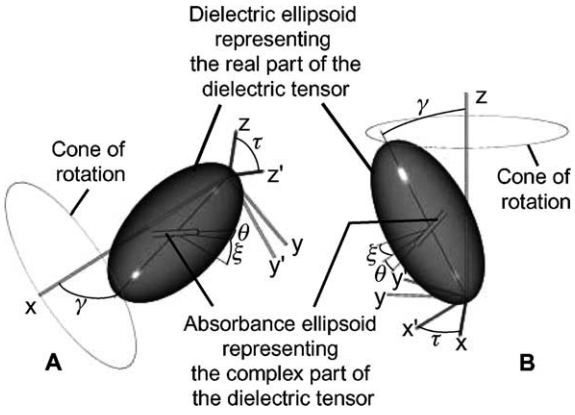

Fig. 1. Coordinate systems used in the derivation of the complex dielectric tensor under conditions of (A) transverse illumination and (B) axial illumination. The shape of larger ellipsoid represents the real part of the dielectric tensor and the smaller cylinder inside depicts the geometric relationship of the complex part of the tensor. The angles θ, ξ and γ represent the tilt of the absorption dipole (Gröbner et al., 2000; Jäger et al., 1997), the rotational diffusion (Brown, 1972) and bilayer tilt (Das, 1995; Liebman et al., 1974; Powers & Nelson, 1995; Roberts et al., 2004) respectively. The rotational degree of freedom in the sample for the whole outer segment around its long axis is set with the angle τ and is shown by the rotation from the x, y', z' axis system to the x, y, z system.

Assuming that the absorption along the long axis of the chromophore is very much greater than the other two orthogonal axes (Mathies & Stryer, 1976), the absorption tensor of the chromophore is given by

$$\boldsymbol{\epsilon} = \begin{pmatrix} 0 & 0 & 0 \\ 0 & \alpha & 0 \\ 0 & 0 & 0 \end{pmatrix}, \tag{2}$$

where α represents the imaginary part of the dielectric constant. However, the main transition dipole of the chromophore is not coincident with the principal axes of the opsin that surrounds it (Gröbner, Burnett, Choi, Mason, & Watts, 2000; Jäger et al., 1997). Therefore, by rotating the chromophore frame of reference into the protein frame by an angle θ (see Fig. 1A), the chromophore tensor in the protein's frame of reference, $\boldsymbol{\epsilon}(\theta)$, becomes

$$\boldsymbol{\epsilon}(\theta) = \mathbf{R}(\theta)\boldsymbol{\epsilon}\mathbf{R}^{-1}(\theta), \tag{3}$$

where

$$\mathbf{R}(\theta) = \begin{pmatrix} \cos\theta & -\sin\theta & 0 \\ \sin\theta & \cos\theta & 0 \\ 0 & 0 & 1 \end{pmatrix}. \tag{4}$$

Multiplying out Eq. (3) and including the real dielectric constants of the protein frame of reference, the full dielectric tensor becomes

$$\boldsymbol{\epsilon}(\theta) = \begin{pmatrix} \epsilon_1 + \alpha\sin^2\theta & -\alpha\sin\theta\cos\theta & 0 \\ -\alpha\sin\theta\cos\theta & \epsilon_2 + \alpha\cos^2\theta & 0 \\ 0 & 0 & \epsilon_3 \end{pmatrix}, \quad (5)$$

where ϵ_i and $i = 1, 2, 3$, represent the three real dielectric constants and $n = \sqrt{\epsilon}$ with n being the refractive index. Also, we set $\epsilon_2 = \epsilon_3$ and define the intrinsic birefringence as $n_1 - n_2$.

Several degrees of freedom must also be accounted for with similar rotational transformations. With reference to the angles defined in Fig. 1A these are: the rotational diffusion of the system (Brown, 1972), ξ; the bilayer tilt (Das, 1995; Liebman et al., 1974; Powers & Nelson, 1995; Roberts, Temple, Haimberger, Gleeson, & Hawryshyn, 2004), γ; and the rotational degree of freedom for the whole outer segment around its long axis, τ. (In Fig. 1A this is the rotation from the x, y', z' axis system to the x, y, z system.) All these parameters can be included in the dielectric tensor for the membrane by similar transformations as in Eq. (3), to give

$$\boldsymbol{\epsilon}(\tau, \gamma, \xi, \theta) = \begin{pmatrix} AA & BB & DD \\ BB & CC & EE \\ DD & EE & FF \end{pmatrix}, \quad (6)$$

where the elements $AA, \ldots, FF$ are defined in Table 1. It is worth noting that the above dielectric tensor is biaxial primarily because the principal axes of the real and complex parts of the tensor are not coincident. However, as will be detailed below, in accounting for the rotational diffusion through the outer segment as a whole, the problem reduces to a uniaxial system.

Under transverse illumination, the form birefringence of the outer segments must also be taken into account. Form birefringence (as opposed to the intrinsic birefringence of the lipid bilayers) occurs due to the ordered arrangement of the membranes where the thickness of the membranes and dimensions of the outer segment are smaller and larger respectively than the wavelength of light. Consideration of the differing boundary conditions when the electric field vector is either parallel or perpendicular to the plane of the membranes then allows the derivation of formulae describing the complex form birefringence. As detailed later, several studies (Harosi, 1981; Laughlin et al., 1975; Liebman, 1975; Liebman et al., 1974; Israelachvili, Sammut, & Snyder, 1975) have theoretically investigated form birefringence with varying degrees of success. In our treatment of this problem, the effect of form birefringence can simply be included within the calculations by generalizing the standard formulations to a tensorial format (Born & Wolf, 1999). For example, if the electric field vector, **E**, is parallel to the plane of the membranes, then its tangential component must be continuous across the surface discontinuity and accordingly (Born & Wolf, 1999, see Sections 15.1 and 15.5)

$$D_k = \sum_l \epsilon_{kl} E_l, \quad (7)$$

where **D** is electric field displacement vector, k stands for the three indices x, y, z, and l stands for each of the x, y and z in turn in the summation. Hence the complex dielectric tensor for light polarized parallel to the plane of the membrane must be given by

$$\boldsymbol{\epsilon}_{\text{transverse}} = f\boldsymbol{\epsilon}(\tau, \gamma, \xi, \theta) + (1 - f)\boldsymbol{\epsilon}_{\text{cytoplasm}}, \quad (8)$$

Table 1
The substitutions used in the derivations of the dielectric tensor for transverse and axial illumination of a photoreceptor

Element	Transverse illumination	Axial illumination
AA	A	$A\cos^2\tau - 2B\cos\tau\sin\tau + C\sin^2\tau$
BB	$B\cos\tau - D\sin\tau$	$B\cos^2\tau - B\sin^2\tau + (A - C)\sin\tau\cos\tau$
CC	$C\cos^2\tau - 2E\cos\tau\sin\tau + F\sin^2\tau$	$A\sin^2\tau + 2B\cos\tau\sin\tau + C\cos^2\tau$
DD	$B\sin\tau + D\cos\tau$	$D\cos\tau - E\sin\tau$
EE	$E\cos^2\tau - E\sin^2\tau + (C - F)\sin\tau\cos\tau$	$D\sin\tau + E\cos\tau$
FF	$C\sin^2\tau + 2E\cos\tau\sin\tau + F\cos^2\tau$	F
A	$a\cos^2\gamma - 2b\cos\gamma\sin\gamma + c\sin^2\gamma$	$a\cos^2\gamma - 2d\cos\gamma\sin\gamma + f\sin^2\gamma$
B	$b\cos^2\gamma - b\sin^2\gamma + (a - c)\sin\gamma\cos\gamma$	$b\cos\gamma - e\sin\gamma$
C	$a\sin^2\gamma + 2b\cos\gamma\sin\gamma + c\cos^2\gamma$	c
D	$d\cos\gamma - e\sin\gamma$	$d\cos^2\gamma - d\sin^2\gamma + (a - f)\sin\gamma\cos\gamma$
E	$d\sin\gamma + e\cos\gamma$	$b\sin\gamma + e\cos\gamma$
F	f	$a\sin^2\gamma + 2d\sin\gamma\cos\gamma + f\cos^2\gamma$
a	$\epsilon_1 + \alpha\sin^2\theta$	$(\epsilon_1 + \alpha\cos^2\theta)\cos^2\xi + \epsilon_2\sin^2\xi$
b	$-\alpha\sin\theta\cos\theta\cos\xi$	$(\epsilon_1 - \epsilon_2 + \alpha\cos^2\theta)\cos\xi\sin\xi$
c	$(\epsilon_2 + \alpha\cos^2\theta)\cos^2\xi + \epsilon_3\sin^2\xi$	$(\epsilon_1 + \alpha\cos^2\theta)\sin^2\xi + \epsilon_2\cos^2\xi$
d	$-\alpha\sin\theta\cos\theta\sin\xi$	$\alpha\cos\theta\sin\theta\cos\xi$
e	$(\epsilon_2 - \epsilon_3 + \alpha\cos^2\theta)\cos\xi\sin\xi$	$\alpha\cos\theta\sin\theta\sin\xi$
f	$(\epsilon_2 + \alpha\cos^2\theta)\sin^2\xi + \epsilon_3\cos^2\xi$	$\epsilon_3 + \alpha\sin^2\theta$

where f is the volume fraction occupied by the bilayers and $\epsilon_{\text{cytoplasm}}$ is the dielectric tensor of the cytoplasm surrounding the bilayers, given by

$$\epsilon_{\text{cytoplasm}} = \begin{pmatrix} \varepsilon & 0 & 0 \\ 0 & \varepsilon & 0 \\ 0 & 0 & \varepsilon \end{pmatrix}, \tag{9}$$

with ε being the dielectric constant of the surrounding cytoplasm. Illumination with with polarized perpendicular to the plane of the membranes follows the same considerations.

By a similar method, the complex dielectric tensor for the membranes under an axial illumination geometry can be derived from the coordinate system illustrated in Fig. 1B. With the change in coordinate system and following a similar series of coordinate transformations, the dielectric tensor for axial illumination is also given by Eq. (6) with the different substitutions, again detailed in Table 1.

From the calculation of the complex dielectric tensors, solutions to Maxwell's equations can be then deduced as set out in several texts, (for example, a detailed derivation in S.I. units is given by Azzam and Bashara (1987)). From the calculation of the single layer optical tensor, solutions to the propagation equation can be obtained, giving the layers' propagation tensor. Under axial illumination, the multiple layered structure of the outer segment can then be correctly modelled through a successive multiplication of the layer propagation tensor with $\epsilon_{\text{cytoplasm}}$ to calculate the overall optic tensor. This also allows rotational diffusion to be accounted for, simply setting the value of ξ with a random number generator (between the limits of 0° and 360°) from one anisotropic layer to the next. However, for transverse illumination, the same layered structure does not exist *along* the direction of propagation. Nevertheless, rotational diffusion must still be taken into account. This is achieved by a similar repeated multiplication of the systems transverse propagation tensor with only the value of ξ changing from one "effective" layer to the next, i.e. the real parts of the tensor are identical through the structure. Finally, generalized field vectors of the external incident, transmitted and reflected waves can be related to the internal electric fields components. This allows both the 2×2 complex amplitude transmission and reflection matrices to be calculated, the determination of which completes the problem.

3. Calculations of photoreceptor absorbance

The accuracy of any theoretical modelling is critically dependent on the validity of the parameters used in the calculation. As described in the previous section, in order to calculate the spectral absorbance of vertebrate photoreceptors under transverse illumination, several physical quantities must be known. The anisotropic real and complex parts of the membrane refractive indices, the refractive index of the cytoplasm surrounding the membranes, the dimensions of the membranes and cytoplasmic space, and the dimensions of the outer segment itself are all required. In the following calculations, we used the previously published value of 1.365 obtained by Liebman et al. (1974) for the refractive index of the cytoplasm. Unfortunately, accurate dispersion data (i.e. the variation of n with wavelength) for outer segment membranes do not exist, in particular data for the complex part of the refractive indices. Liebman et al. (1974) and Liebman (1975) measured the intrinsic birefringence and mean value of the real part of the membrane refractive indices to be 0.0135 and 1.475 respectively. From these results, $n_{\parallel} = 1.481$ and $n_{\perp} = 1.468$ represent a good approximation for the refractive indices. Here $n_{\parallel}$ and $n_{\perp}$ signify the refractive indices parallel and perpendicular to the mean molecular orientation in the membrane. These values are also consistent with calculations in Israelachvili et al. (1975). The complex dispersion in the membrane refractive indices was estimated from the results of Chance, Perry, Akerman, and Thorell (1959) and Harosi (1981). Fig. 2A illustrates the function used to model the complex dispersion. In this study we only considered the α- and β-absorption bands, with the function a sum of two Gaussian distributions. In order to calculate the relative wavelength position of the β band, we used the equation for A1 pigments derived by Govardovskii, Fyhrquist, Reuter, Kuzmin, and Donner (2000),

$$\lambda_{\max\beta} = 189 + 0.315\lambda_{\max\alpha} \tag{10}$$

where $\lambda_{\max\beta}$ and $\lambda_{\max\alpha}$ are the wavelengths of maximum absorbance for the β and α bands respectively. It is worth noting that the value of the complex dispersion at $\lambda_{\max\alpha}$ is $\approx 16\times10^{-4}$, a close approximation to the value of 13.5×10^{-4} calculated by Harosi (1981). The value of θ for the tilt of the chromophore dipole moment was 16° (Jäger et al., 1997). Dimensions of the outer segment membranes and surrounding cytoplasm were modelled as 200 and 100 Å respectively and were included in the calculation of the transverse propagation tensor to account for the form birefringence.

In order to make comparisons between our work and experimental measurements, the calculations in the rest of this paper consider transverse illumination, as this is the typical experimental illumination geometry. Examples of calculated axial absorbance spectra have been published elsewhere (Roberts et al., 2004). Fig. 2B illustrates calculated absorbance spectra for a model UVS cone, rod and LWS cone photoreceptor at absorbance maxima of 372, 505 and 575 nm respectively. In these calculations the outer segment diameters were modelled to be 3 μm. Qualitatively, the profiles of the curves are typical of absorbance spectra measured

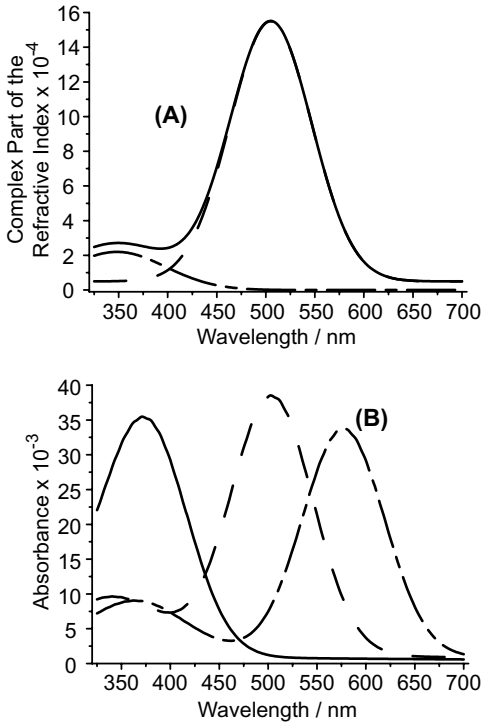

Fig. 2. (A) Two Gaussian distributions (dashed lines) summed to model the complex dispersion relation (solid line) in membrane dielectric tensor. (B) Example calculated absorbance spectra for a UVS cone (solid line, $\lambda_{max} = 372$ nm), a rod (dashed line, $\lambda_{max} = 505$ nm) and a LWS cone (dashed–dotted line, $\lambda_{max} = 575$ nm). Parameters used for the calculations are described in the text.

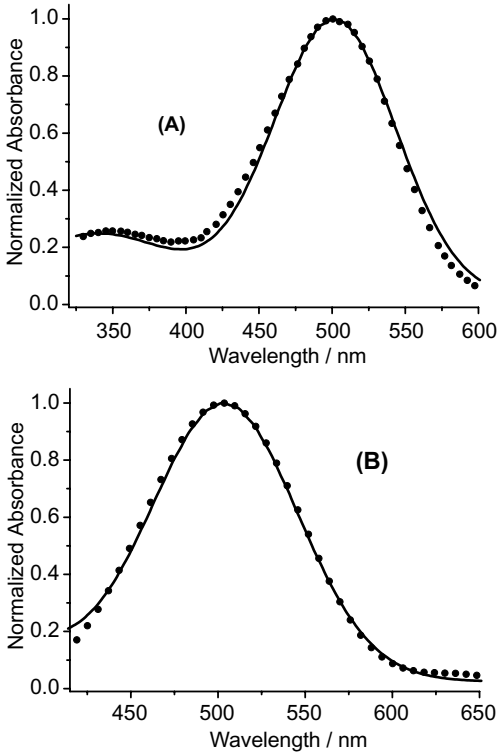

Fig. 3. Comparisons between experimentally measured (filled squares) and calculated (solid line) rod absorbance spectra. (A) experimental data of *Bufo bufo* measured by Govardovskii et al. (2000, redrawn from Fig. 1C) and (B) experimental data of *O. kisutch* measured by Roberts et al. (2004).

experimentally by microspectrophotometry (MSP), clearly showing both the α- and β-absorbance bands. Quantitatively, the magnitudes of absorbance also compare well to experimental results. For the modelled rod, the absorbance at λ_{max} was approximately 38×10^{-3} for a 3 μm diameter outer segment. This equates to a specific absorbance of 0.013 OD, which lies within 0.008–0.017 OD, the range generally measured across a wide variety of vertebrate species (Harosi, 1981; Harosi & MacNichol, 1974b; Hawryshyn, Haimberger, & Deutschlander, 2001).

To further investigate how closely the profiles of our calculations agreed with experimental MSP measurements, we directly compared our results with experimental absorbance spectra of rods from (Fig. 3A) *Bufo bufo* (Govardovskii et al., 2000, redrawn from Fig. 1C) and (Fig. 3B) *Oncorhynchus kisutch* (Roberts et al., 2004). In order to calculate the absorbance spectra with a similar λ_{max} to the experimental results, we choose $\lambda_{max\alpha}$ of the complex part of the refractive index accordingly. Both sets of calculated data were also normalized to account for the unknown outer segment diameters. Considering the assumption associated with the complex refractive index dispersion, the comparison between spectra is remarkably good. The deviations between the calculated and experimental measured spectra can be solely attributed to the Gaussian form of the modelled complex dispersion not accurately describing the exact physiological function. Interestingly in Fig. 3A there is a 2 nm difference between calculated and experimental $\lambda_{max\beta}$. This indicates that while the relationship of Govardovskii et al. (2000) set out in Eq. (10) is accurate for the A1 absorbance spectra template, it does not directly translate to the complex dispersion in the dielectric tensor.

4. The absorbance spectrum profile

Eq. (1) defined how the absorbance is calculated as decadic logarithm of the transmittance. However, this formula is only strictly valid when there is no loss (reflection or scattering) within the sample. Experimentally, it is always assumed that these losses are negligible. Nevertheless, for light travelling through inhomogeneous media with multiple refractive index changes, this must be considered to be an approximation.

A common feature of many published experimental absorbance spectra has been the elevated nature of the short-wavelength side of the spectrum. The rise in the measured absorbance can occur for several reasons, with photoproduct production being perhaps the most

common. However, in studies where bleaching and photoproduct production have been effectively minimized, a rise in absorbance at shorter wavelengths is often still seen. Fig. 4A illustrates this with a typical example of such an absorbance curve redrawn from Harosi (1987, Fig. 3). It is generally understood that scattering effects and the numerical aperture mismatch between condenser and objective contribute to this type of spectrum profile. Within our calculations, we can make similar assumptions to the experimental situation by ignoring any reflections and simply calculating the absorbance as $\log\frac{1}{T}$ where we have unit incident intensity and T is the transmitted intensity. Such a calculation is presented in Fig. 4B, and clearly shows a similar artifact of the raised absorbance at shorter wavelengths.

Several published MSP studies have paid particular attention to the reduction of these experimental losses. Most notable is perhaps the recent study of Govardovskii et al. (2000, see Appendix 2) on the validity of universal visual pigment template. Fig. 3A, (Govardovskii et al., 2000, redrawn from Fig. 1C) showed that with careful control of experimental losses and the benefit of the large diameter outer segments of *Bufo bufo*, experimental absorbance measurements produce absorbance spectra without the elevated absorbance at shorter wavelengths. Indeed, they concluded that MSP rod absorbance spectra match almost exactly the digitonin extract spectra from the same species. In accounting for any loses, our calculations (Fig. 3A solid line) also produced minimal distortion on the short-wavelength side of the spectrum. This leads therefore to a general conclusion that such elevation in the absorbance (when there is minimal photoproduct production) is primarily an experimental artifact due to loss within the sample.

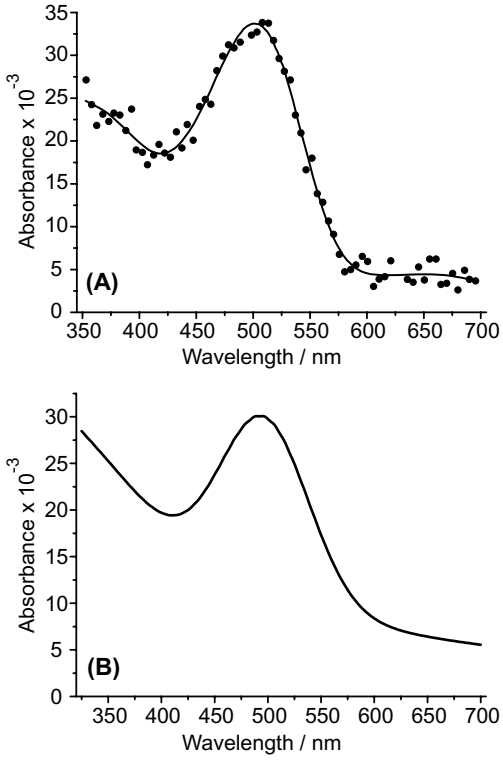

Fig. 4. Absorbance spectra, (A) experimental (measured by Harosi (1987, redrawn from Fig. 3)) and (B) calculated, both showing elevated absorbance at shorter wavelengths due to the assumption of no reflection in the system. Note the line in (A) is from the original figure and is not a calculation from this work.

5. Calculations of dichroic ratios

In studying photoreceptor optics, several workers, for example Liebman (1962), Harosi and MacNichol (1974a, 1974b), Harosi (1987), have made measurements of the dichroic ratio, DR. As mentioned in the introduction, the DR is the ratio of absorbance parallel and perpendicular to the transverse axis of the photoreceptor (Harosi & Malerba, 1975) and such measurements have been used in the proposal of several models for the ordered distribution of rhodopsin within rod outer segments (Harosi & Malerba, 1975; Liebman, 1962). The general treatment of the problem by Harosi and Malerba (1975) resulted in the conclusion that the main transition dipole is inclined at an angle of 16°–18° to the transverse axis of the outer segment, a fact more recently confirmed using NMR measurements (Gröbner et al., 2000; Jäger et al., 1997). The original motivation behind Harosi's work was to correctly account for the effects of the condenser numerical aperture (N.A.) in DR measurements since, as they point out, the light microscope could not fulfil its job as an optical magnifier if it were to use collimated light. Their calculations (Harosi & Malerba, 1975, Fig. 3) showed that the value of the DR was a strong function of the N.A. reducing for example from 200 to 10 when increasing the N.A. from 0.2 to 0.8. However, in assessing the importance of the N.A., the analysis presented did not include the tilt of the chromophore transition dipole moment calculated in the work. Using Eq. (10) from Harosi and Malerba (1975) we have reproduced the dependence of the DR on the condenser N.A. (Fig. 5), but for the situation when the transition dipole moment of the chromophore is both tilted (at 16°, the solid line) and not tilted (the dashed line and previously calculated by Harosi and Malerba (1975)) with respect to the plane of the membrane. It can be clearly seen from this calculation that the measured DR is in fact a much weaker function of the N.A. when the tilt of the transition dipole of the chromophore is considered. The dichroic ratio is only reduced from 6.4 to 4.5 when increasing the N.A. from 0.2 to 0.8. Nevertheless, the effect of the convergent incident beam does reduce the measured DR at high numerical apertures.

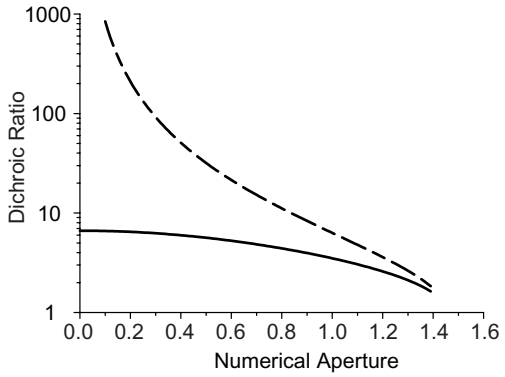

Fig. 5. Calculated dichroic ratios as a function of the system condenser numerical aperture, after Harosi and MacNichol (1974a). The dashed and solid lines represent the chromophore transition dipole moment orientation parallel to the transverse axis of the outer segment and tilted at an angle of 16° (Harosi & MacNichol, 1974a; Liebman, 1962).

We can similarly calculate the DRs from first principles and for the first time analyze theoretically how the DR changes as a function of both wavelength and the photoreceptor dispersion. A further benefit of our analysis is that we fully incorporate the effects of form birefringence into the calculations. Various other works (Harosi, 1981; Israelachvili et al., 1975; Laughlin et al., 1975; Liebman, 1975; Liebman et al., 1974) have attempted to theoretically calculate this effect of form birefringence, although none offer a complete description. For example previous works such as Israelachvili et al. (1975), Harosi (1981) predicted a strong form birefringence component for the membrane volume fraction equal to zero. Of course if their are no membranes and the system is isotropic, there can be no form birefringence. Also, nearly all previous works ignored the anisotropic nature of the membranes themselves (with the exception of Israelachvili et al. (1975)). To the authors' knowledge no other work has also attempted to account for the correct geometry of the complex part of the refractive indices. A more complete study of the effects of form birefringence on the DR of vertebrate photoreceptors will be the subject of a future publication by the authors.

In Fig. 6A two calculated absorbance curves are presented where the incident light is polarized parallel (solid line) and perpendicular (dashed line) to the transverse axis of the outer segment. Experimentally measured DR values are generally quoted at the λ_{max} value, which

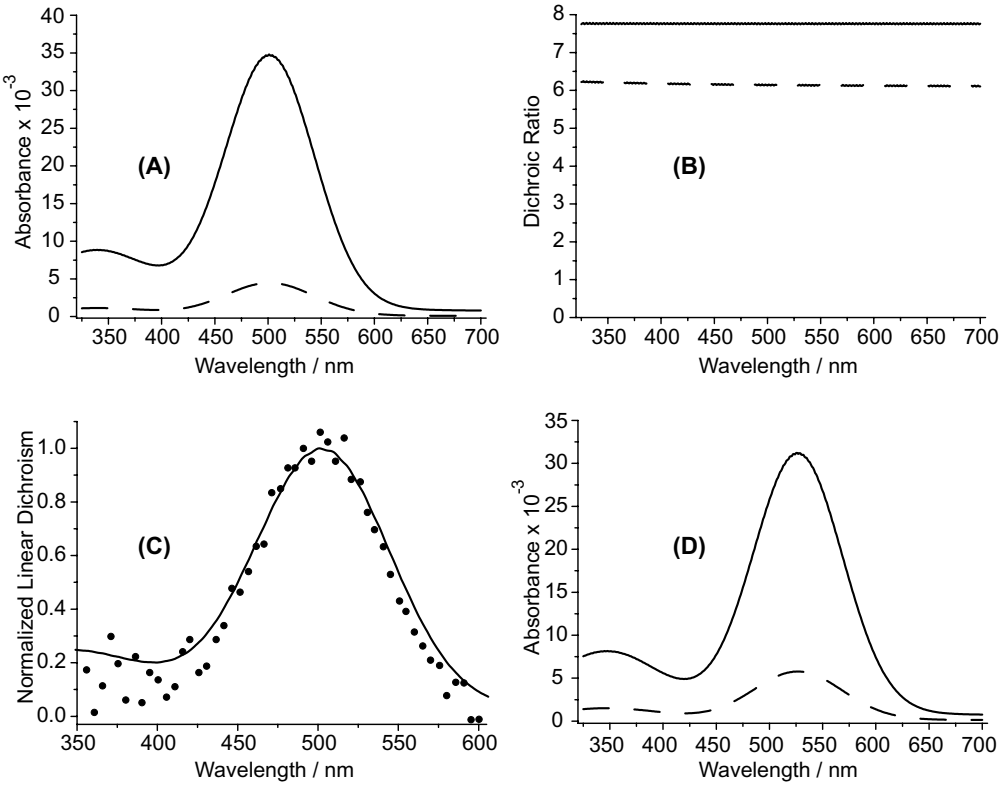

Fig. 6. (A) Calculated absorbance spectra for a rod, where the solid and dashed lines signify the absorbance for linearly polarized light parallel and perpendicular to the transverse axis of the outer segment. (B) The dichroic ratio calculated from (A) as a function of wavelength ignoring (dashed line) or accounting for (solid line) form birefringence. Dichroic ratios are seen to be independent of wavelength. (C) Linear dichroism calculated from (A, solid line) compared directly with experimental results (filled circles) of Harosi (1987, redrawn from Fig. 2B). (D) Calculated orthogonal absorbance spectra for a MWS cone including the tilted optical geometry measured by Roberts et al. (2004).

results in a calculated value for the rod depicted here of 7.7 (parameters used were as for the rod in Fig 2B). In fact Fig. 6B shows that the DR is independent of wavelength, a result which agrees with Palacios, Srivastava, and Goldsmith (1998), who found the DR to be an constant function of wavelength in photoreceptors of several species of amphibian. The two curves in Fig. 6B represent the calculated DR when the form birefringence is included (solid line, $f = 0.3$ (Israelachvili et al., 1975)) or ignored (dashed line) in the calculations. It can clearly be seen that the effect of form birefringence increases the DR by a factor of 1.26. This again is similar to previously published results. Table 2 presents several examples of experimental DR measurements from a variety of animals, and as can be seen from this table, values for vertebrate rods typically lie in the range of 3–5. Therefore, although our calculated value is the correct order of magnitude, it does appear somewhat too high. However, in our model we have only considered collimated incident light and not the convergent beam used in experiments, and as discussed previously, correcting for a typical condenser N.A. would reduce our calculated results ≈5.5 much closer to experimental measurements. Also, we should again consider the experimental approximation of no losses within the system. Calculating the DR of the absorbance spectra where the reflected component was ignored (Fig. 4B) gives a value of ≈4 when no form birefringence is considered. Consequently, the combination of the form birefringence, effect of the numerical aperture and the somewhat unquantifiable nature of the loss in the system would result in the calculated DR lying in experimentally measured range of 3–5. One should perhaps conclude from this discussion that it appears somewhat fortuitous the effects of form birefringence and loss within the system effectively cancel out, such that Liebman (1962) and Harosi and Malerba (1975) actually calculated the correct tilt of the main transition dipole. As a further comparison, in a study of all spectral classes of photoreceptors from two species of monkey (*Maccaca fasicularis* and *M. mulatta*), Harosi (1987) measured the linear dichroism as a function of wavelength, an equivalent parameter to the DR defined as proportional to $(T_{\parallel} - T_{\perp})/(T_{\parallel} + T_{\perp})$. Converting our results to linear dichroism and normalizing both sets of data, (Fig. 6C) shows they are in excellent agreement with each other.

One consistent finding for dichroism measurements of vertebrate photoreceptors has been that cones posses a lower DR than rods. Table 2 gives several examples of cone measurements and typically the DR range is 2–3, compared to 3–5 for rods. Several explanations have been put forward for this difference. For example, Harosi and MacNichol (1974b) suggested a direct relationship between the cell size and the measured DR values, citing increased refraction and loss due to the smaller radii of curvature. However, cones and rods of similar diameters still exhibit the same trend between their DRs. A further possibility is that recent experimental results (Roberts et al., 2004) showed that rod and cone photoreceptors in coho salmon (*O. kisutch*) absorb linearly polarized light differently. All spectral classes of cone (and not rods) were found to exhibit a tilted optical geometry where the maximum absorbance of transversely illuminating polarized light occurred when the

Table 2
Previously measured dichroic ratios

Dichroic Ratio	Photoreceptor type	Species	Reference
5.3	Rod	*Rana pipiens*	Liebman (1962)
5	Rod	*Rana pipiens*	Harosi (1971)
3.9–4.9	Rod	*Rana pipiens*	Harosi and MacNichol (1974a)
4.55	Rod	*Ambystoma tigrinum*	Harosi (1975)
3.12	Rod	*Necturus maculosus*	Harosi (1975)
4.1	Rod	*Rana temporaria*	Bowmaker (1977)
3.2	Rod	*Tribolodon hakonensis*	Harosi and Hashimoto (1983)
2.68–3.77	Rod	*Macaca fascicularis*	Harosi (1987)
3	Rod	*Tupaia belangeri*	Petry and Harosi (1990)
3.1	Rod	*Rana pipiens* and *Ambystoma tigrinum*	Palacios et al. (1998)[a]
4.6	Rod	*Rana ridibunda*	Govardovskii et al. (2000)
2–3	Cones	9 species of fish	Svaetichin et al. (1965)[b]
2–3	SWS, MWS and LWS cones	*Carassius auratus*	Harosi and MacNichol (1974b)
1.33–1.52	SWS, MWS and LWS cones	*Macaca fascicularis*	Harosi (1987)
1.25–1.34	MWS and LWS cones	*Macaca mulatto*	Harosi (1987)
1.8–2.5	Cones	*Tribolodon hakonensis*	Harosi and Hashimoto (1983)
2.1–2.2	LWS cones	*Tupaia belangeri*	Petry and Harosi (1990)
2.8	UV cones	*Cyprinus carpio*	Hawryshyn and Harosi (1991)
2.2–3.2	UV cones	*Gecko Gecko*	Loew (1994)

[a] The dichroic ratio was measured using a suction pipette technique not microspectrophotometrically, as in all other cases in this table.
[b] Values quoted by Harosi (1981).

E-vector was not parallel to the transverse axis of the outer segment. This result was not due to the tilt of the chromophore transition dipole. All rods measured exhibited maximum absorbance only for light polarized parallel to the transverse axis of the photoreceptor, the expected result considering rotational diffusion and the mean molecular orientation normal to the plane of the membrane. In our calculations of absorbance in cones, we accounted for the tilt through the parameter γ (see Fig. 1) and set the magnitude to 15°. This represented a conservative value based on the experimentally measured distribution. Fig. 6D shows that with accounting for form birefringence in a MWS cone calculation, the difference between the orthogonal absorbance curves, and therefore the DR is visibly reduced and at λ_{max} the DR is ≈5. Again considering the effect of numerical apertures within the system and the assumption of no loss, the value becomes consistent with the range of experimental measurements in Table 2. As yet the origin of the tilted optical structure in this species is undetermined, although Roberts et al. (2004) proposed two possibilities; either the membranes are tilted with respect to the outer segment or the mean molecular orientation within the membranes is tilted with respect to the layer normal. Work is currently being undertaken to resolve these possibilities. Nevertheless, entertaining the possibility that a similar tilted optical geometry may exist in the cones of other species offers an accurate explanation of the difference between the dichroic ratios of rods and cones.

6. Conclusions

In summary, we have presented analytic solutions to Maxwell's equations for a physiologically accurate model of rod and cone photoreceptors. By using previously measured optical parameters, such as refractive indices or the orientation of the main transition dipole within the cell, we have shown that the calculated absorbance spectra match experimental results to very good level of agreement. The validity of this approach allowed us to assess the accuracy of the general experimental assumption that no reflection or scattering occurs in the sample during MSP measurements. Our results proved that a commonly observed artifact of increased measured absorbance at shorter wavelengths can be due entirely to this assumption. MSP has also been consistently used to measure dichroic ratios of photoreceptors. By correctly accounting for the effects of form birefringence, numerical apertures within the system and again the assumption of no loss, we find that the calculations accurately predict measured dichroic ratios. Furthermore, the dichroic ratios of cones are always measured to be less than those of rods. Incorporating the findings of Roberts et al. (2004) into the model resulted in the correct prediction of a lower dichroic ratio in vertebrate cones.

Acknowledgments

The financial support of the Engineering and Physical Sciences Research Council and Royal Society is acknowledged. The authors also wish to thank C.W. Hawryshyn and S.E. Temple for many valuable discussions.

References

Azzam, R. M., & Bashara, N. M. (1987). Ellipsometry and polarised light. Amsterdam: Elsevier (p. 340).

Berreman, D. W. (1972). 4×4 matrix methods. *Journal of the Optical Society of America, 62*(4), 502.

Born, M., & Wolf, E. (1999). Principles of optics (7th ed.). Cambridge: Cambridge University Press (p. 837).

Bowmaker, J. (1977). Long lived photoproducts of the green-rod pigment of the frog, *Rana Temporaria*. *Vision Research, 17*, 17–23.

Brown, P. (1972). Rhodopsin rotates in the visual receptor membrane. *Nature New Biology, 236*, 35.

Chance, B., Perry, R., Akerman, L., & Thorell, B. (1959). Highly sensitive recording microspectrphotometer. *Review of Scientific Instruments, 30*, 735–741.

Das, P. (1995). Solitons in cell membranes. *Physical Review E, 51*(4), 3588–3612.

Denton, E. J. (1958). *Visual problems of colour* (Vol. 1). London: Her Majesty's Stationary Office (pp. 175–188).

Govardovskii, V. I., Fyhrquist, F., Reuter, T., Kuzmin, D. G., & Donner, K. (2000). In search of the visual pigment template. *Visual Neuroscience, 17*, 509–528.

Gröbner, G., Burnett, C. G., Choi, A., Mason, J., & Watts, A. (2000). Observations of light-induced structural changes of retinal within rhodopsin. *Nature, 405*, 801–813.

Harosi, F. I. (1971). *Frog rhodopsin in situ: orientational and spectral changes in the chromophores of isolated retinal rod cells*. Ph.D. thesis, John Hopkins University, Baltimore, MD, USA.

Harosi, F. I. (1975). Linear dichroism of rods and cones. In M. A. Ali (Ed.), *Vision in fishes: new approaches in research. NATO advanced study institute series. Series A life sciences* (Vol. 1). New York, London: Plenum Press (pp. 55–65).

Harosi, F. I. (1981). Microspectrophotometry and optical phenomena: birefringence, dichroism and anomalous dispersion. In J. M. Enoch & F. L. Tobey (Eds.), *Vertebrate photoreceptor optics* (pp. 337). Berlin: Springer-Verlag.

Harosi, F. I. (1987). Cynomolgus and Rhesus monkey visual pigments: Application of Fourier transform smoothing and statistical techniques to the determination of spectral parameters. *Journal of General Physiology, 89*, 717–743.

Harosi, F. I., & Hashimoto, Y. (1983). Ultraviolet visual pigment in a vertebrate: A tetra-chromatic cone system in the dace. *Science, 222*, 1021–1023.

Harosi, F. I., & MacNichol, E. F. (1974a). Dichroic microspectrophotometer: a computer assisted, rapid, wavelength scanning photometer for measuring the linear dichroism of single cells. *Journal of the Optical Society of America, 64*, 903–918.

Harosi, F. I., & MacNichol, E. F. (1974b). Visual pigments of goldfish cones. Spectral properties and dichroism. *Journal of General Physiology, 63*, 279–304.

Harosi, F. I., & Malerba, F. E. (1975). Plane polarized light in microspectrophotometry. *Vision Research, 15*, 379–388.

Hawryshyn, C. W., Haimberger, T. J., & Deutschlander, M. E. (2001). Microspectrophotometric measurements of vertebrate photoreceptors using CCD-based detection technology. *Journal of Experimental Biology, 204*, 2431–2438.

Hawryshyn, C. W., & Harosi, F. I. (1991). Ultraviolet photoreception in carp: Microspectrophotometric and behaviourally determined action spectra. *Vision Research, 31*, 567–576.

Israelachvili, J. N., Sammut, R. A., & Snyder, A. W. (1975). Birefringence and dichroism of photoreceptors. *Vision Research, 16*, 47–52.

Jäger, S., Lewis, J. W., Zvyaga, T. A., Szundi, I., Sakmar, T. P., & Kliger, D. S. (1997). Chromophore structural changes in rhodopsin from nanoseconds to microseconds following pigment photolysis. *Proceedings of the National Academy of Sciences of the United States of America, 94*, 8557–8562.

Laughlin, S. B., Menzel, R., & Snyder, A. W. (1975). Membranes, dichroism and receptor sensitivity. In A. W. Snyder & R. Menzel (Eds.), *Photoreceptor optics* (pp. 237). Berlin: Springer-Verlag.

Liebman, P. A. (1962). *In situ* microspectrophotometric studies on the pigments of single retinal rods. *Biophysical Journal, 2*, 161–178.

Liebman, P. A. (1975). Birefringence, dichroism and rod outer segment structure. In A. W. Snyder & R. Menzel (Eds.), *Photoreceptor optics* (pp. 119). Berlin: Springer-Verlag.

Liebman, P. A., Jagger, W. S., Kaplan, M. W., & Bargoot, F. G. (1974). Membrane structure changes in rod outer segments with rhodopsin bleaching. *Nature, 251*, 31–36.

Loew, E. R. (1994). A third ultraviolet-sensitive visual pigment in the Tokay Gecko (*Gecko Gecko*). *Vision Research, 34*, 1427–1431.

Mathies, R., & Stryer, L. (1976). Retinal has a highly dipolar vertically excited singlet state: implications for vision. *Proceedings of the National Academy of Sciences of the United States of America, 73*(7), 2169–2173.

Palacios, A. G., Srivastava, R., & Goldsmith, T. H. (1998). Spectral and polarization sensitivity of photocurrents of amphibian rods in the visible and ultraviolet. *Visual Neuroscience, 15*, 319–331.

Petry, H. M., & Harosi, F. I. (1990). Visual pigments of the tree shrew (*Tupaia belangeri*) and greater galago (*Galago crassicaudatus*): A microspectrophotometric investigation. *Vision Research, 30*, 839–851.

Powers, T., & Nelson, P. (1995). Fluctuating membranes with tilt order. *Journal de Physique II, 5*(11), 1671–1678.

Roberts, N. W., Bowring, N., Gleeson, H. F., Seed, A., Nassif, L., Hird, M., & Goodby, J. (2003). Physical properties and reflection spectra of SmC^* sub-phases. *Journal of Materials Chemistry, 13*, 353–359.

Roberts, N. W., Temple, S. E., Haimberger, T. J., Gleeson, H. F., & Hawryshyn, C. W. (2004). Differences in the optical properties of vertebrate photoreceptor classes leading to axial polarization sensitivity. *Journal of the Optical Society of America*, 1–11.

Schmidt, W. J. (1938). Polarisationsoptische analyse eines eiweiss-lipoid-systems, erläutert am aussenglied der sehzellen. *Kolloideitschrift, 85*, 137–148.

Snyder, A. W. (1979). *Physics of vision in compound eyes. Handbook of sensory physiology* (Vol. VII/6A). Berlin, Heidelberg, New York: Springer (pp. 225–314).

StJohn, W. D., Fritz, W. J., Lu, Z. J., & Yang, D. K. (1995). Bragg reflection from cholesteric liquid crystals. *Physical Review E, 51*(2), 1191–1198.

Svaetichin, G. K., Negishi, K., & Fatehchand, R. (1965). Cellular mechanisms of a Young–Hering visual system. In A. V. S. DeReuck & J. Knight (Eds.), *Ciba foundation symposium on colour vision: physiology and experimental psychology* (pp. 178–207). Boston: Little, Brown and Company.

Weale, R. A. (1971). On the linear dichroism of frog rods. *Vision Research, 11*, 1373–1385.